JGR Biogeosciences

RESEARCH ARTICLE
10.1029/2022JG007156

Moving Bedforms Control CO_2 Production and Distribution in Sandy River Sediments

H. Schulz[1,2], Y. Teitelbaum[3], J. Lewandowski[1,2], G. A. Singer[1,4], and S. Arnon[3]

[1]Department Ecohydrology and Biogeochemistry, Leibniz Institute of Freshwater Ecology and Inland Fisheries, Berlin, Germany, [2]Geography Department, Humboldt University of Berlin, Berlin, Germany, [3]Zuckerberg Institute for Water Research, The Jacob Blaustein Institutes for Desert Research, Ben-Gurion University of the Negev, Beersheba, Israel, [4]Department of Ecology, University of Innsbruck, Innsbruck, Austria

Abstract Streams and rivers play an important role in the global carbon cycle. The origins of CO_2 in streams are often poorly constrained or neglected, which is especially true for CO_2 originating from heterotrophic metabolism in streambeds. We hypothesized that sediment movement will have a direct effect on stream metabolism, and thus, the aim of this study was to quantify the effect of moving bedforms on the production of CO_2 in sandy streambeds. We conducted flume experiments where we used planar optodes to measure the distributions of O_2 and CO_2 under various streambed celerities. We combined these measurements with an assessment of bed morphodynamics and modeling to calculate O_2 consumption and CO_2 production rates. Our results indicate that sediment transport can strongly influence streambed metabolism and CO_2 production. We found that bedform celerity controls the shape of the hyporheic zone and exchange flux, and is directly linked to the spatial and temporal distributions of O_2 and CO_2. It was also found that the most pronounced change in CO_2 production occurred when the bed changed from stationary conditions to a slowly moving bed. A more gradual increase in O_2 consumption and CO_2 production rates was observed with further increase in celerity. Our study also points out that bedform movement causes hydraulic isolation between the moving and the non-moving fraction of the streambed that can lead to a transient storage of CO_2 in deeper sediments, which may be released in bursts during bed scour.

Plain Language Summary Streams play an important role in the global carbon cycle. Carbon is transported in streams and rivers toward the oceans, stored in the streambed, or emitted as the greenhouse gas CO_2 to the atmosphere. Many studies try to link CO_2 in streamwater and CO_2 emission to flow conditions and CO_2 import via groundwater while ignoring the role of microbial processes in sediments that also produce CO_2. We performed lab experiments using an artificial stream channel and special sensors in the streambed to investigate the influence of moving sandy sediments on the distribution and production of CO_2. We found that sediment movement controls the distribution of CO_2, and that those distributions are influenced by the flow paths of the water flowing through the sediment. We also found that the production of CO_2 and the flux of stream water entering the sediment increased with the speed of the sediment movement. Moreover, our results point out that the movement of the sediment disconnects the lower, non-moving part of the sediment from the upper, moving part of the sediment. This can build up a storage of high CO_2 concentrations in the deeper sediment, which may be released as bursts during events of streambed erosion.

Key Points:

- Bedform celerity controls the spatial and temporal distribution of CO_2 in stationary and moving sandy bedforms
- Production of CO_2 in sediments increases abruptly as the bed starts to move and more gradually with increasing bedform celerity
- Bedform movement causes isolation of the non-moving fraction of the streambed and increase in transient storage of CO_2 in deeper sediments

Supporting Information:

Supporting Information may be found in the online version of this article.

Correspondence to:

H. Schulz,
h.schulz@igb-berlin.de

Citation:

Schulz, H., Teitelbaum, Y., Lewandowski, J., Singer, G. A., & Arnon, S. (2023). Moving bedforms control CO_2 production and distribution in sandy river sediments. *Journal of Geophysical Research: Biogeosciences*, *128*, e2022JG007156. https://doi.org/10.1029/2022JG007156

Received 9 SEP 2022
Accepted 24 MAR 2023

Author Contributions:

Conceptualization: H. Schulz, J. Lewandowski, G. A. Singer, S. Arnon
Data curation: H. Schulz
Formal analysis: H. Schulz, S. Arnon
Funding acquisition: H. Schulz, J. Lewandowski, G. A. Singer
Investigation: H. Schulz, Y. Teitelbaum
Methodology: H. Schulz, Y. Teitelbaum, G. A. Singer, S. Arnon
Project Administration: H. Schulz, J. Lewandowski, G. A. Singer, S. Arnon
Resources: J. Lewandowski, G. A. Singer, S. Arnon

1. Introduction

Freshwater systems play an important role in the global carbon (C) cycle (Battin et al., 2009). The C originating from terrestrial sources is stored in aquatic sediments, exported to the ocean, or evaded to the atmosphere in the form of CO_2 (Cole et al., 2007; Raymond et al., 2013; Regnier et al., 2013). Most research on CO_2 evasion from rivers considers the river system as a "black box" where origins of CO_2 are often poorly constrained or neglected (Marx et al., 2017; Peter et al., 2014; Saccardi & Winnick, 2021).

The relative contribution of external versus internal sources of CO_2 to the overall pool in the stream is highly variable and depends mostly on river size (Hotchkiss et al., 2015), the position along the river continuum from headwaters to estuary (Lauerwald et al., 2015), as well as seasonal discharge alterations (Finlay, 2003; Gu et al., 2021), catchment geology (Rovelli et al., 2022), and rates of C transformation (Hotchkiss et al., 2015). Gaseous CO_2 in the atmosphere is in equilibrium with dissolved CO_2 in the water, and the exchange between

Software: H. Schulz, Y. Teitelbaum
Supervision: J. Lewandowski, G. A. Singer, S. Arnon
Validation: H. Schulz, Y. Teitelbaum
Visualization: H. Schulz
Writing – original draft: H. Schulz, S. Arnon
Writing – review & editing: Y. Teitelbaum, J. Lewandowski, G. A. Singer, S. Arnon

them is determined by Henry's Law. Dissolved CO_2, together with bicarbonate (HCO_3^-) and carbonate (CO_3^{2-}), comprises the pool of dissolved inorganic carbon (DIC) (Stumm & Morgan, 1996). The fractionation of DIC between the aforementioned species depends on pH and temperature (Jones Jr. et al., 2003; Marx et al., 2017). In-stream CO_2 is controlled by CO_2 exchange with the atmosphere, in-stream metabolic processes, and input from external sources (Hope et al., 2004; Stumm & Morgan, 1996). The latter includes the import of CO_2 via shallow groundwater exfiltration that originates from root respiration, soil organic matter decomposition, soil CO_2 dissolution, and carbonate weathering (Amiotte-Suchet et al., 1999; Ge et al., 2021; Hope et al., 2004). On the one hand, several studies report the external input of CO_2 as the major contributor to the overall pool in the water column of rivers and streams (Gu et al., 2021; Peter et al., 2014; Rovelli et al., 2022). On the other hand, the importance of in-stream metabolism to the overall CO_2 evasion was also found to be substantial (Finlay, 2003; Rasilo et al., 2017; Saccardi & Winnick, 2021).

Stream metabolism is characterized by complex interactions between hydrological, chemical, and biological processes. Despite increasing numbers of measurements and improved sensor technologies, it is challenging to identify spatial patterns or to build reliable predictive models for metabolism (Bernhardt et al., 2018). It was reported that in-stream metabolism contributes to the concentration of CO_2 in the water column mostly by respiration of aquatic plants and heterotrophic respiration of organic matter (Crawford & Stanley, 2016; Hope et al., 2004). Heterotrophic respiration occurs mostly in the streambed. For instance, Naegeli and Uehlinger (1997) estimated the contribution of streambed respiration at 76%–96%, and Fellows et al. (2001) to 40%–93% of the overall stream ecosystem respiration. Others even found that most of the observed metabolism originated from plankton (Oliver & Merrick, 2006). In terms of overall catchment CO_2 evasion, Saccardi and Winnick (2021) determined that the contribution of the benthic sediment layer and water column were 50.6% and 0.1%, respectively, and Hotchkiss et al. (2015) found that in-stream metabolism was responsible for 28% of the total evasion.

Formation of CO_2 in the streambed by heterotrophic activity and its evasion from streamwater depends on particular hydrological conditions. Nutrients and oxygen need to be delivered from the streamwater into the sediments where C transformation occurs, and CO_2 has to be delivered back to the streamwater from which it is eventually emitted to the atmosphere. The aforementioned active zone in the sediment is commonly called the hyporheic zone (HZ). For brevity, we refer to the HZ as the area of the streambed sediment in which pore water flow paths originate and end at the sediment-water interface, while hyporheic exchange (HE) describes the water exchange between streamwater and sediment, and the flux through the HZ is referred to as hyporheic exchange flux (HEF) (Fox et al., 2014; Gooseff, 2010; Harvey et al., 1996). HEF is driven by the irregular shape of the water-sediment interface and the pressure distribution at that interface. It can be lateral due to meanders or vertical due to submerged structures such as bedforms (Gomez-Velez & Harvey, 2014; Hutchinson & Webster, 1998; Zheng et al., 2019). Bedform-driven HEF controls the exchange rates of solutes between the stream and the streambed. Thus, HEF influenced various biogeochemical reactions and was used to model nutrient dynamics at larger scales, such as for a catchment scale (Gomez-Velez et al., 2015; Gomez-Velez & Harvey, 2014).

Bedform movement and biogeochemical processes in streambeds have been studied extensively, but mostly independently (Boano et al., 2014; Lewandowski et al., 2019; Mueller et al., 2022). Only recently have studies on biogeochemical processes emerged that started to unravel complex interactions between flow conditions, bed movement, and nutrient dynamics. For example, modeling studies suggested that rapid bedform movement forms a well-mixed oxic surface layer in the upper fraction of the sediment (Ahmerkamp et al., 2015; Kessler et al., 2015; Zheng et al., 2019). Thus, a redox seal is created between the well-mixed aerated zone and the anoxic sediments below (Precht et al., 2004). HE is strongly impacted by the movement of the bedform, where an increase in celerity flattens the flow paths and increases the exchange due to the movement of the bed (turnover) as compared to the exchange due to advection (pumping) (Elliott & Brooks, 1997a; Packman & Brooks, 2001).

Several experimental studies on respiration were conducted in the last few years. For example, Ahmerkamp et al. (2017) observed a 50% reduction of oxygen consumption rates in a batch experiment with sand from moving bedforms as compared to sand from stationary bedforms. They also conducted measurements of oxygen and celerity in sea sediment. By combining the observation with a mathematical model, it was revealed that consumption rates tend to decrease with celerity. However, they tested only a narrow range of water velocities and bedform celerities that are typical for marine sediments (0–4.9 cm h^{-1}). In another study, Scheidweiler et al. (2021) found that phototrophic and heterotrophic microbial activity was reduced in the moving sediment as compared to the stationary sediment. In the latter study, only mechanical stress due to physical abrasion, habitable

area, and light limitation was examined, and the effect of pore water transport processes could not be evaluated since the experiments were done in agitated batch chambers. The only experimental study that systematically evaluated the effect of celerity on oxygen consumption was done by Wolke et al. (2019). They tested the rates of oxygen consumption under a wide range of celerities (0–67 cm h^{-1}) and found that rates tend to slightly decline as celerity increases. To further investigate the dynamics of metabolism under moving bedforms, the objective of the present study was to quantify the effect of moving bedforms on the production of CO_2 in sandy streambeds. We refer to the streambed as one unit that may have a moving and non-moving fraction, depending on the flow condition. We hypothesized that an increase in streamwater velocity and bedform celerity will (a) alter the zones of biogeochemical activity and, hence, the distribution of CO_2 in the sediment, and (b) result in a decrease of CO_2 production in the streambed.

2. Materials and Methods

2.1. Study Design

Experiments were conducted in a recirculating flume, packed with natural sediments, where we quantified the consumption of O_2 as well as the production of CO_2 in the streambed using planar optode measurements under different streamwater velocities and bedform celerities. We used six different streamwater velocities that ranged between 12 and 37 cm s^{-1}). In each experimental run, the streamwater velocity was adjusted approximately 12 hr before the measurements of O_2, CO_2, and pH with planar optodes. Experimental runs lasted approximately 6 hr. In total, we tested 12 runs under six different flow conditions in two sets (Figure S1 and Table S2 in Supporting Information S1). In addition, we conducted experiments for physical characterization of the system under each of the flow conditions. These included (a) measurements of bedform celerity, height, and length, (b) velocity profiling near the streambed to calculate shear velocities, and (c) dye tracer tests to visualize HE. A numerical model was used to calculate the HEF (Teitelbaum et al., 2022). Furthermore, gas tracer tests were conducted to determine the evasion of CO_2 from the streamwater to the atmosphere under all tested velocities.

2.2. Experimental Setup

Natural sediment was collected from the upper 10 cm of the streambed of the Yarqon Stream, an urban stream in central Israel (Arnon et al., 2015) (Figures S2a and S2b in Supporting Information S1). The sediment was taken to the laboratory where it was wet sieved with a 2-mm mesh. Material that did not pass the sieve, such as gravel, pieces of wood, and shells, was discarded. Afterward, the sieved sediment was aerated for 2 days by frequent manual mixing while keeping it moist. The sediment was packed in the channel of the flume under water while ensuring homogeneity by hand mixing during the packing (Figure S2c in Supporting Information S1). The final bed height was approximately 17 cm and the bed covered an area of 260×29 cm^2 of the channel. A ramp made from an impermeable plastic sheet was installed in the first 60 cm from the inlet of the channel as a transition zone to reach the bed height (Figure 1a and Figure S2c in Supporting Information S1).

The flume was filled with deionized water and flushed three times to reduce the amount of fine suspended sediment in the water column. DI water was chosen as a working fluid to allow repeatability of the experiments. The option of using streamwater from the Yarqon Stream was not feasible due to the large volumes required. The stream water was circulated for an adaptation time of 11 days before the start of the experiments to allow for stabilization between water and sediment. Previous studies using the same flume setup did not find an effect of DI water on the microbial community in the sediment (De Falco et al., 2018). To overcome the potential effect of changing water chemistry (e.g., reduction of available DOC over time), and to make sure that there was no other systematic effect due to the applied conditions, we conducted the experiments in two sets with six streamwater velocities in random order. Sodium chloride (NaCl) was added to the water to reach an electrical conductivity (EC) of approximately 1.5 mS cm^{-1} to increase the stability and life-time of the CO_2 planar optodes. This is similar to the EC in the Yarqon Stream during the summer (unpublished data). The flow in the flume was controlled with a variable-speed centrifugal pump that was able to recirculate the transported sediment, while a magnetic flow meter (SITRANS F M, MAG 5100 W S, Nordborg, Denmark) was used to measure discharge. Average velocity was calculated by dividing the discharge by the cross-sectional area of the water column. The cross-sectional area was determined by multiplying the width of the flume by the average water depth. The average water depth was calculated from depth measurements taken at a 5-cm interval along a 60-cm section in the middle of the flume. A side loop of water recirculation was used to drive water through a chiller (TR/TC 10, TECO Refrigeration Technologies, Ravenna, Italy) to keep the temperature

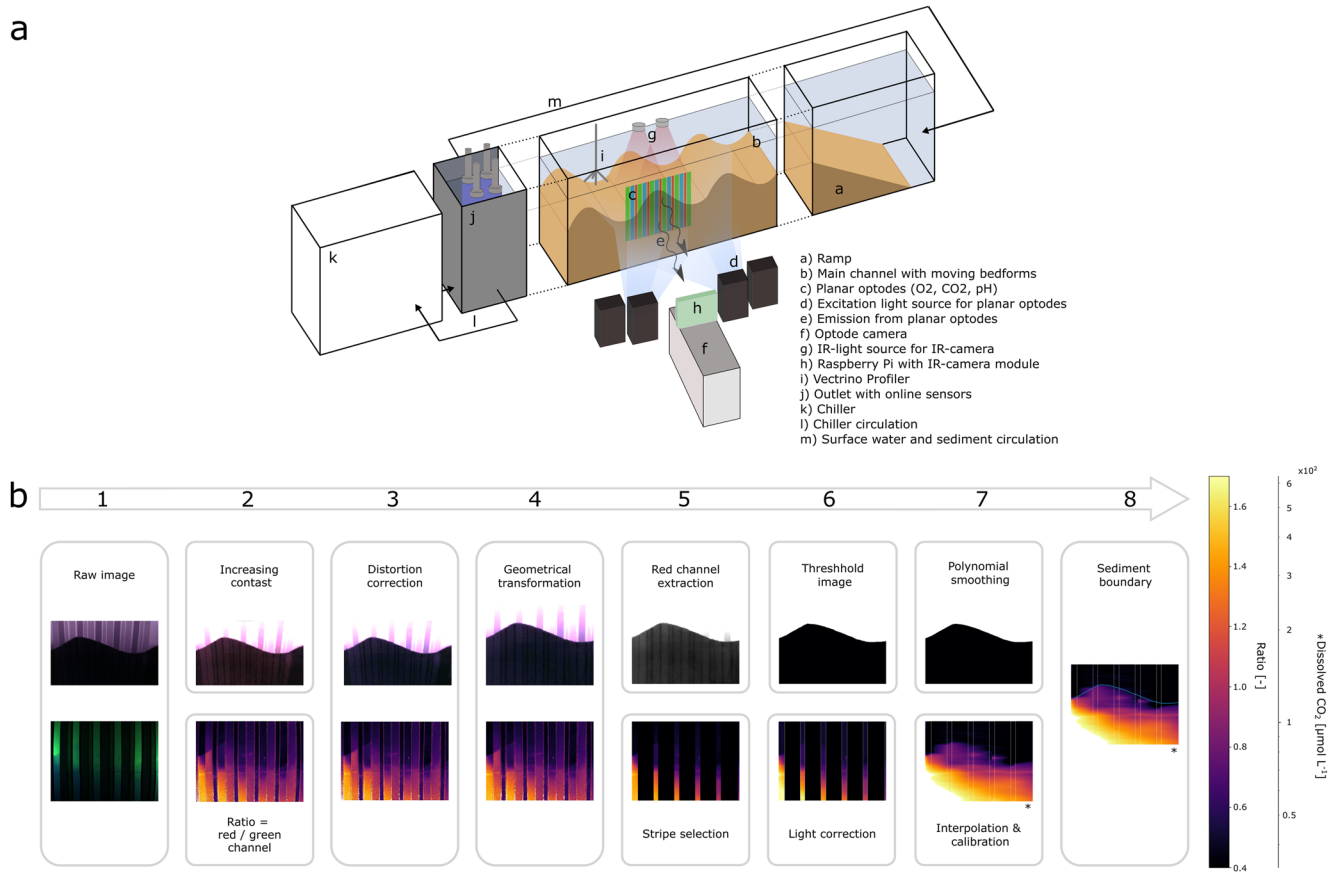

Figure 1. (a) Schematic presentation of experimental flume setup to investigate moving bedforms with planar optodes, and (b) simplified scheme of preprocessing steps involved to reach final calibrated images from planar optodes. The first row shows steps involved for infrared (IR) images that were used to detect the streamwater sediment interface and the shape of the bedforms. The second row shows the preprocessing steps for CO_2 optode images. Images in steps 2–6 show concentrations in form of ratios between red and green color channels. Images of steps 7 and 8 show calibrated concentrations on a log-scale indicated by *.

between 24.5 and 25.0°C. The top of the flume was open to allow gas exchange. A pavilion of black fabric was placed over the flume to avoid algal growth and photosynthesis, and to protect the photosensitive planar optodes.

Hydraulic conductivity, organic matter content, and porosity of the bed were determined at the beginning and at the end of the entire experiment. Due to manual mixing of the sediment during the packing process, the sediment was homogeneous in the beginning of the experiment (Figure S2c in Supporting Information S1). At the end of the experiment, sediment of the moving (upper few centimeters) and the stationary bed fractions were sampled and analyzed separately (Figure S2d in Supporting Information S1). The porosity was determined according to standard procedures by weighing and drying saturated sediments at 105°C. The organic fraction of the sediment was determined as loss on ignition (450°C for 4 hr) of five replicates. Hydraulic conductivity and median grain size diameter D_{50} were determined by characterizing the particle size distribution of the bed using 12 sieves with mesh sizes between 0.053 and 1.68 mm, followed by an analysis with HydrogeoSieveXL v2.3.2 using the method by Hazen (Devlin, 2016).

2.3. Hydrological and Chemical Characterization

Dye tracer tests were performed using Brilliant Blue dye to visualize HE under all six streamwater velocities. About 20 g of dye dissolved in 5 L deionized water was added to the streamwater and images were taken perpendicular to the flow direction through the glass wall of the flume every minute for 10 hr by a digital camera (Nikon D5300, with AF-P DX NIKKOR 18–55 mm VR Lens, Ayuthaya, Thailand).

HEF was calculated with a numerical model (Teitelbaum et al., 2022). Briefly, the model describes the movement of periodic mobile bedforms within a fixed modeling frame. The model uses a sinusoidal pressure boundary condition at the bed surface, exponentially attenuated head versus depth at the left and right boundaries of the

domain, and a no-flux boundary condition along the bottom of the domain (Elliott & Brooks, 1997b). Hydraulic head in the bed is computed using the steady-state groundwater flow equation, and pore water flow paths are computed using Darcy's Law. More information about the model can be found in Teitelbaum et al. (2022) and Text S1 in Supporting Information S1.

2.3.1. Sediment Morphodynamics

Velocity profiles near the water-sediment interface were measured using an acoustic doppler velocimeter (Vectrino Profiler, Nortek, Rud, Norway). The velocimeter was installed at a fixed distance above the crest of a bedform. Velocities were determined in 1 mm intervals for the first cm above the streambed and with 1 cm intervals in the rest of the water column. Shear velocity was calculated from velocity profiles above the streambed by fitting a logarithmic profile and determined for four streamwater velocities (19, 24, 29, and 34 cm d^{-1}). Missing values were calculated via linear interpolation.

Bedform length and celerity were calculated using the time-lapse images from the dye tracer experiments. We used Python codes to detect the streamwater sediment interface, to locate the troughs of the bedforms passing through the image by applying SciPy's "find_peaks" function (Virtanen et al., 2020), and used those troughs to determine bedform lengths and celerities. Celerity is determined from the position change of troughs as they move horizontally through the time-lapse images (Dallmann et al., 2020; Teitelbaum et al., 2021).

Bedform height was measured by fixing an acoustic profiler (Nortek Vectrino II Profiler, Rud, Norway) above the sediment in the water column and continuously measuring the distance to the bed as it moved below. The troughs and peaks of the bedforms are also computed using the SciPy's "find_peaks" function. The function finds troughs and peaks of the bedforms passing below the sensor to determine their height. A minimum prominence level of 5 cm was set to exclude small streambed height variations that would otherwise be detected as bedforms.

2.3.2. Streamwater Chemistry

Sensors for measuring pH (PHEHT) and O_2 (OPTOD, Aqualabo, Champigny sur Marne, France), and CO_2 (eosGP, Eosense, Dartmouth, Canada) were installed in the channel of the flume to measure the values of these parameters in the streamwater with a sampling interval of 1 min. The data from the sensors were collected with a CR1000 data logger (Campbell Scientific, USA). A handheld meter (WTW, Multi 3420, Weilheim, Germany) was used to check the calibration of the sensors on a daily basis and to ensure constant EC. Grab samples were taken from the streamwater for analysis of dissolved (DOC) and total (TOC) organic carbon (Analytik Jena, multi N/C 2100 S, Jena, Germany), nutrients levels by using spectrophotometric methods (Tecan Trading, Spark 10M, Männedorf, Switzerland), cation concentrations (AMETEK, SPECTRO ARCOS, Kleve, Germany), and alkalinity (Metrohm, 775 Dosimat, Herisau, Switzerland). Alkalinity was determined by titration with 0.01 M.HCL. All data are available in Table S3 in Supporting Information S1 and Table S4. DIC was calculated based on dissolved CO_2 concentration and daily alkalinity values (Section 2.5.1). Additionally, saturation indices were calculated using the software PHREEQC version 3 to assess whether the use of DI water as a working fluid was causing an undersaturation of common carbonates (Parkhurst & Appelo, 2013).

2.3.3. CO_2 Evasion

CO_2 evasion was calculated by multiplying the gas transfer velocity k_{CO2} with the difference between CO_2 concentration measured in the streamwater (C_{SW}) and Air (C_{Air}) (Equation 1).

$$F = k_{CO2} \cdot (C_{SW} - C_{Air}) \quad (1)$$

C_{Air} was measured using a CO_2 sensor (K30, Senseair AB, Delsbo, Sweden). Mounting and calibration of the sensor were done following the instructions by Bastviken et al. (2015). The concentration of the streamwater was measured using the sensor eosGP (eosGP, Eosense, Dartmouth, Canada). Both gas sensors report CO_2 as a molar fraction (xCO_2, in ppm) in a gaseous phase. To translate xCO_2 to an aqueous concentration of CO_2, we followed Henry's law using atmospheric pressure in the laboratory and a Henry coefficient adjusted to the water temperature ($C = xCO_2 \cdot 10^{-6} \cdot P_{atm}/K_H$).

k_{CO2} was calculated using Equation 2 where $k600$ is the gas transfer velocity with a Schmidt number of 600 and Sc_{CO2} is the Schmidt number of CO_2.

$$k_{CO2} = k_{600} \cdot \left(\frac{Sc_{CO2}}{600}\right)^{-0.5} \quad (2)$$

The Schmidt number is the ratio of the kinematic viscosity of water to the diffusion coefficient at given temperatures T (in °C): $Sc_{CO2} = A + B \cdot T + C \cdot T^2 + D \cdot T^3$; using coefficients A, B, C, and D from Raymond et al. (2012). $k600$, was determined from gas tracer tests using dissolved oxygen measurements conducted at six streamwater velocities in duplicate. For the gas tracer test, the water column of the flume was covered with a plastic foil to prevent gas exchange with the atmosphere. The water was cooled down from approximately 25–20°C. Afterward, the foil was removed to allow oxygen release from the streamwater to the atmosphere. An online O_2 sensor (OPTOD, Aqualabo, Champigny sur Marne, France) was used to measure O_2 as it adapted to the saturation concentrations at the new temperature. Detailed calculations of k600 from the resulting O_2 curves are provided (Text S2 in Supporting Information S1).

2.4. Solute Imaging

A planar optode system was used to measure the spatial distribution of CO_2, O_2, and pH at the sediment-water interface (VisiSensTD, Presens GmbH, Regensburg, Germany). Self-adhesive optodes (CO_2: SF-CD1R; O_2: SF-RPSU4; pH: SF-HP5R) were cut in 1-cm wide stripes (0.5-cm wide for pH optodes) of 15 cm length. These were installed in vertical orientation in an alternating way at the inner side of the flume before packing the sediment (Figure 1a). Approximately a 2-mm distance between stripes was kept to avoid light disturbance by adjacent stripes. A total of six stripes of CO_2 optodes, five of O_2 and five of pH covered a total area of 16.5 × 15 cm^2. Excitation light sources (VisiSens TD Big Area Imaging Kit, Presens GmbH, Regensburg, Germany) and the optode camera were placed perpendicular to the flume 17 cm away from the optodes. To align the optode measurements with bedforms, the bed was imaged using an infrared (IR) camera module operated by a Raspberry Pi (Raspberry Pi 4 model b, Raspberry Pi foundation, United Kingdom). IR LEDs were installed on the top of the flume to increase the contrast between streamwater and streambed. Excitation and IR light sources were switched on and off sequentially and automatically when images were taken. IR time-lapse images were taken every minute for the duration of optode measurements (approximately 6 hr). The sampling rate of planar optode images varied with bedform celerity and was chosen in a way to capture moving bedforms while minimizing the number of images. This was done as exposure to excitation light sources may lead to photodegradation of the planar optodes.

2.4.1. Image Preprocessing

Matching between the position of the sediment-water interface to the various optode images was done by using the Open Source Computer Vision Library (OpenCV) (Bradski, 2000), as shown in Figure 1b. As a first step, the contrast of the IR images needed to be increased and the brightness adjusted to prepare the images for the later boundary extraction. Next, a distortion correction of the images was applied by taking pictures of a chess board and determining distortion coefficients according to the chessboard's distortion using the OpenCV library (step 2 in Figure 1b). The determined distortion coefficients were then used to undistort the images taken throughout the experiments (Bradski, 2000; Singh, 2019). Thereafter, the IR image was resized and corrected for trapeze distortion by placing a frame (11 × 15 cm^2) on top of the optodes. This frame made it also possible to overlay IR and planar optode images during the final processing step. Furthermore, the red channel was extracted to create a gray scale image for threshold determination. The threshold value was needed to determine a binary image that displays the streamwater sediment interface (step 5). For that, images were smoothed by Gaussian blur and the threshold value was determined by trial and error. Finally, the interface between the streamwater and the sediment was extracted from the binary threshold images and smoothed by polynomial filtering using the savgol_filter function of Python's Scipy package.

For the preprocessing of the optode images, the first step was to divide the red channel by the green channel, as suggested by the manufacturer, to create a gray scale image presenting the non-calibrated raw data shown in Figure 1b (step 2). A distortion and geometric transformation were performed in accordance with the IR image preprocessing described above. Raw data of the stripes was blurred by averaging surrounding cells with a window of 20 pixels. A light correction was applied to account for unequal excitation light distribution in CO_2 and pH optodes (description in Figure S4 in Supporting Information S1). Missing data between stripes was interpolated by linear grid interpolation using Scipy's griddata function. The raw data was calibrated with daily calibration curves for O_2 and CO_2 and a single calibration curve for pH optodes. As a final step, the streamwater sediment boundary extracted from IR images was placed on top of the optode images. Image processing and related calculations were done using Python.

2.4.2. Calibration

Daily calibration curves for CO_2 optodes were calculated based on experimentally determined weekly calibration curves. Experimentally determined calibration of the CO_2 optodes was done by using pieces of planar optodes of the same production batch that were installed in a calibration chamber, which was then filled with streamwater from the flume. The CO_2 sensor (eosGP, Eosense, Dartmouth, Canada) was placed in the calibration chamber while the water temperature was kept constant at 25°C. A magnetic stirrer ensured constant mixing while a 9% standard CO_2 gas was added to the water for 30 s through a bubbling stone. Afterward, CO_2 images were taken every 30 min for at least 12 hr. The data of the eosGP were corrected for air and water pressure, transformed to dissolved concentrations by following the instructions provided by the manufacturer, and matched to their corresponding optode images. The calibration data were fitted to a sigmoid function (Equation 3)

$$y = -\left(B + \frac{A + B}{1 + 10^{\frac{x - x_0}{d_x}}}\right) + 2 \cdot k \tag{3}$$

where A is the curve's maximum value, B is the curve's minimum value, x_0 is the function's midpoint on the x-axis, k is the function's midpoint on the y-axis, and d_x is the steepness of the function. In between weekly calibrations, the calibration chamber was placed close to the planar optode setup in the flume to ensure comparable light exposure of optodes installed in the flume and calibration chamber. Measurements from the sensor drifted over time due to inherent bleaching of the optodes; thus, we calculated daily calibration curves for every measurement day assuming a linear drift of the optodes between weekly experimental calibrations (Figure S5 in Supporting Information S1).

Planar oxygen optodes were calibrated on a daily basis by linear regression using a two-point calibration. The value for 100% oxygen saturation was determined by an area of 20 × 20 pixels of the optode positioned in the streamwater. In addition, the value for 0% by anoxic area of equal size in the deepest section of the stationary sediment. This section of the sediment was considered to be anoxic based on characteristic oxygen profiles in the sediment (Figure 4) and previous experiments with oxygen microsensors confirming anoxic conditions in the deeper sediments using a similar experimental setup (De Falco et al., 2016, 2018). Planar pH optodes were calibrated with 10 buffer solutions of different pH (5.4–8.4) after all experimental runs had been completed. The calibration data points were fitted to a sigmoid function (Equation 4; Brodersen et al. (2017)) where A is the curve's maximum value, B is the curve's minimum value, x_0 is the function's midpoint on the x-axis, and d_x is the steepness of the function. The pH calibration curve was offset-corrected using streamwater pH data collected by the pH sensor (see Section 2.3.2).

$$y = B + \frac{A + B}{1 + 10^{\frac{x - x_0}{d_x}}} \tag{4}$$

2.5. Data Analysis

2.5.1. Dissolved Inorganic Carbon

DIC in aquatic systems may be abundant in the form of several components of the carbonate system, whose relative proportions are dependent on the pH (Jones Jr. et al., 2003; Marx et al., 2017). DIC was calculated using the python package PyCO2SYS version 1.8.1 (Humphreys, Sandborn, et al., 2022) developed by Humphreys, Lewis, et al. (2022) for carbonate system calculations in marine environments. It was calculated from CO_2 distributions and alkalinity determined from daily streamwater samples. PyCO2SYS requires concentrations of sulfate, phosphate, ammonia, calcium, fluoride, and salinity as input to the model (Input parameters in Table S2 in Supporting Information S1). In addition, the model requires the values of pH, alkalinity, and atmospheric and hydrostatic pressure. In that way, input parameters are adjusted for every CO_2 optode image analyzed. The model output is a simple translation of CO_2 distribution into DIC distribution (Figure S6 in Supporting Information S1).

2.5.2. Respiration Rates and Reactive Transport

Respiration rates in the streambed were calculated based on the oxic area of the sediment. The oxic sediment area $A_{t,oxic}$ in the planar optode images was defined as the pixels within the sediment whose individual oxygen

Table 1
Hydrological Conditions During the Experiments

Streamwater velocity [cm s^{-1}]	Shear velocity [cm s^{-1}]	Bedform celerity [cm h^{-1}]	Bedform height [cm]	Bedform length [cm]	HEF total [cm d^{-1}]	HEF pumping [cm d^{-1}]	HEF turnover [cm d^{-1}]	Damkoehler number [–]
12	0.5	0	1.2	11.1	8	8	0	75
21	0.7	4	1.4	13.0	23	19	4	18
25	0.9	13	1.4	14.4	32	22	10	10
30	1.4	54	1.4	15.5	58	19	39	6
32	1.8	71	1.5	18.4	64	17	47	6
37	2.6	121	1.6	19.3	98	18	80	4

Note. All values are arithmetic means of the entire data set of a specific velocity.

concentration at time t ($C_{t,i}$) was greater than 10% (Equation 5). About 10% was used as an arbitrary threshold as it best delineates the oxic area that was observed in the optode.

$$|P_{Ox,t}| = \{P_i : C_{t,i} \geq 10\%\} \tag{5}$$

where P_i is the ith pixel. The number of oxic pixels $|P_{Ox,t}|$ was multiplied by the pixel size $A_{pix} = 0.00012$ cm^2 to obtain $A_{t,oxic}$:

$$A_{t,oxic} = A_{pix} \cdot |P_{Ox,t}| \tag{6}$$

The mean concentration $\overline{C}_{t,A_{oxic}}$ of O_2 at time t was calculated from data points within the oxic area of the sediment using Equation 7. Concentrations of individual pixels $C_{t,i}$ within $P_{Ox,t}$ were summed up and divided by the number of oxic pixels $|P_{Ox,t}|$ (Equation 7). The mean concentration of CO_2 in the sediment was calculated similarly to Equations 5–7.

$$\overline{C}_{t,A_{oxic}} = \frac{1}{|P_{Ox,t}|} \sum_{P_{Ox,t}} C_{t,i} \tag{7}$$

Solute mass fluxes into and out of the sediment for each instant ($F_{t,in}$ and $F_{t,out}$) were calculated by Equation 8. Fluxes were based on mean concentrations in the streamwater $\left(\overline{C}_{t,sw}\right)$ and in the oxic zone of the sediment $\left(\overline{C}_{t,A_{oxic}}\right)$ for in- and outfluxes, respectively. The solute mean concentration was multiplied by the HEF (q_h), which describes the mean flux of water entering and leaving the streambed, of the respective streamwater velocity (Table 1). Using the mean of the concentration in the sediment and the mean HEF is a simplified approach to calculate the outflux. This simplification is chosen, because current models cannot capture the spatial and temporal variability of bedform sizes and shapes that passed through the measurement zone.

$$F_{t,in} = \overline{C}_{t,sw} \cdot q_h \qquad and \qquad F_{t,out} = \overline{C}_{t,A_{oxic}} \cdot q_h \tag{8}$$

Oxygen consumption rates ($R_{t,O2}$) were determined for each time point using the delta method (Wolke et al., 2019) and were based on the difference between F_{in} and F_{out}, and divided by the sediment's porosity and the mean oxygen penetration depth ($\delta = A_{t,oxic}/W_{optode}$) (Equation 9). Production rates for CO_2 and DIC ($R_{t,CO2/DIC}$) were calculated in a similar way but swapping subtrahend and minuend (Equation 10). This approach assumes that the concentration difference between stream and pore water is due to respiration only.

$$R_{t,O2} = \frac{F_{t,in\_O2} - F_{t,out\_O2}}{\delta \cdot \theta \cdot 24h} \tag{9}$$

$$R_{t,CO2/DIC} = \frac{F_{t,out\_CO2/DIC} - F_{t,in\_CO2/DIC}}{\delta \cdot \theta \cdot 24h} \tag{10}$$

The respiratory quotient (RQ) is the molar ratio of the amount of CO_2 produced to the amount of O_2 consumed during respiration (Pennington et al., 2018). It was calculated by dividing $R_{t,DIC}$ by $R_{t,O2}$ for each point in time t (Equation 11). $R_{t,DIC}$ was chosen to calculate RQ to include all the inorganic carbon produced in the system.

$$RQ = \frac{R_{t,DIC}}{R_{t,O2}} \tag{11}$$

The non-dimensional Damkoehler number (Da) was used to relate the timescales of oxygen consumption rates (τ_r) to oxygen transport (τ_{tr}) in the streambed (Equation 12), where λ is the bedform wavelength, U_p is a characteristic pore water velocity, R_{O2} the oxygen consumption rate of the streambed, and $C_{O2,sw}$ the concentration of the streamwater. Transport dominates at $Da \ll 1$, whereas reaction rates dominate at $Da \gg 1$ (Ahmerkamp et al., 2017).

$$Da = \frac{\tau_{tr}}{\tau_r} = \frac{\lambda}{U_p} \frac{R_{O2}}{C_{O2,sw}} \tag{12}$$

3. Results

3.1. Hydrology, Morphodynamics, and Streamwater Chemistry

The sediment used in the flume experiments was classified as medium sand. Only the upper few centimeters of the sediment moved due to streamwater flow. At the end of the experiment, the moving fraction of the bed had a slightly higher porosity ($\Theta = 0.4$) and slightly larger median grain size diameter ($d_{50} = 0.28$ mm) as compared to the non-moving fraction ($\Theta = 0.38$; $d_{50} = 0.26$ mm). The calculated hydraulic conductivity, K_s, at the end of the experimental runs was $4.9 \cdot 10^{-4}$ and $4.5 \cdot 10^{-4}$ m s^{-1} for the moving and non-moving fraction, respectively. The mean organic matter content of sediment samples taken in the beginning and in the end of the experiment was 0.58%.

Streamwater velocities of experimental runs ranged from 12 to 37 cm s^{-1} while water depth was maintained at 14 cm. Bedform celerities and HEF increased non-linearly with increasing streamwater velocity (Table 1 and Figure S7a in Supporting Information S1). HEF increased abruptly as soon as the sediment started to move, but a further increase of HEF with celerity was relatively linear (Table 1 and Figure S7b in Supporting Information S1). Advective pumping was solely responsible for HEF in stationary streambeds. Advective pumping increased until the water velocity reached 30 cm s^{-1}, and remained relatively constant with further increase in velocity. This occurred due to the increase in bedform length and decrease in bedform height, which balanced the expected increase in pressure due to the increasing water velocities. Turnover contributed increasingly to the total HEF as celerity increases, and reached up to 82% of the total HEF at a celerity of 1.21 m h^{-1}. Damkoehler number was the highest in stationary streambeds. It decreased substantially as soon as the sediments started to move, and more gradually with further increase in celerity.

Oxygen measurements using online sensors showed 100% air saturation throughout experimental runs. CO_2 concentrations in the streamwater ranged between 553 and 660 ppm (Table 1) and were positively correlated with streamwater velocity. The general water chemistry resembled the water chemistry of the Yarqon Stream (Tables S1 and S3 in Supporting Information S1 and Table S4). Saturation indices of common carbonates indicated a saturation or a slight oversaturation already within the initial days after the flume setup (Figure S3 in Supporting Information S1 and Table S5). This indicates that rapid chemical stability occurred in the initial days following the flume setup, and before the metabolism measurements started. A slight increase in nutrients was observed during the experiments (Table S3 in Supporting Information S1, Table S4, and Table S5), because of the mineral dissolution and due to the continuous sediment movement under high celerities.

3.2. Hyporheic Exchange

HE was visualized with time-lapse images of dye tracer penetration into the bed under different celerities (Figure 2). For brevity, we refer to the area that participated in the exchange, that is, subsurface area covered with blue dye, as the HZ. In addition, we could visually differentiate between the moving and non-moving fractions of the bed. The moving fraction, which contained more coarse-grained sediment, lay on top of the non-moving fraction, whose sediment was more homogeneous and yellowish in color. This clear visual interface, that is, the deepest scour level indicated by a white dashed line in Figure 2, is the result of the passage of many bedforms and does not necessarily imply the current interface between the moving and non-moving fractions. Clear visual evidence of the moving and non-moving fractions, which issued from previous faster flow conditions when the bed moved, also appears in the images of the stationary streambed ($c = 0$ m h^{-1}). Under stationary conditions,

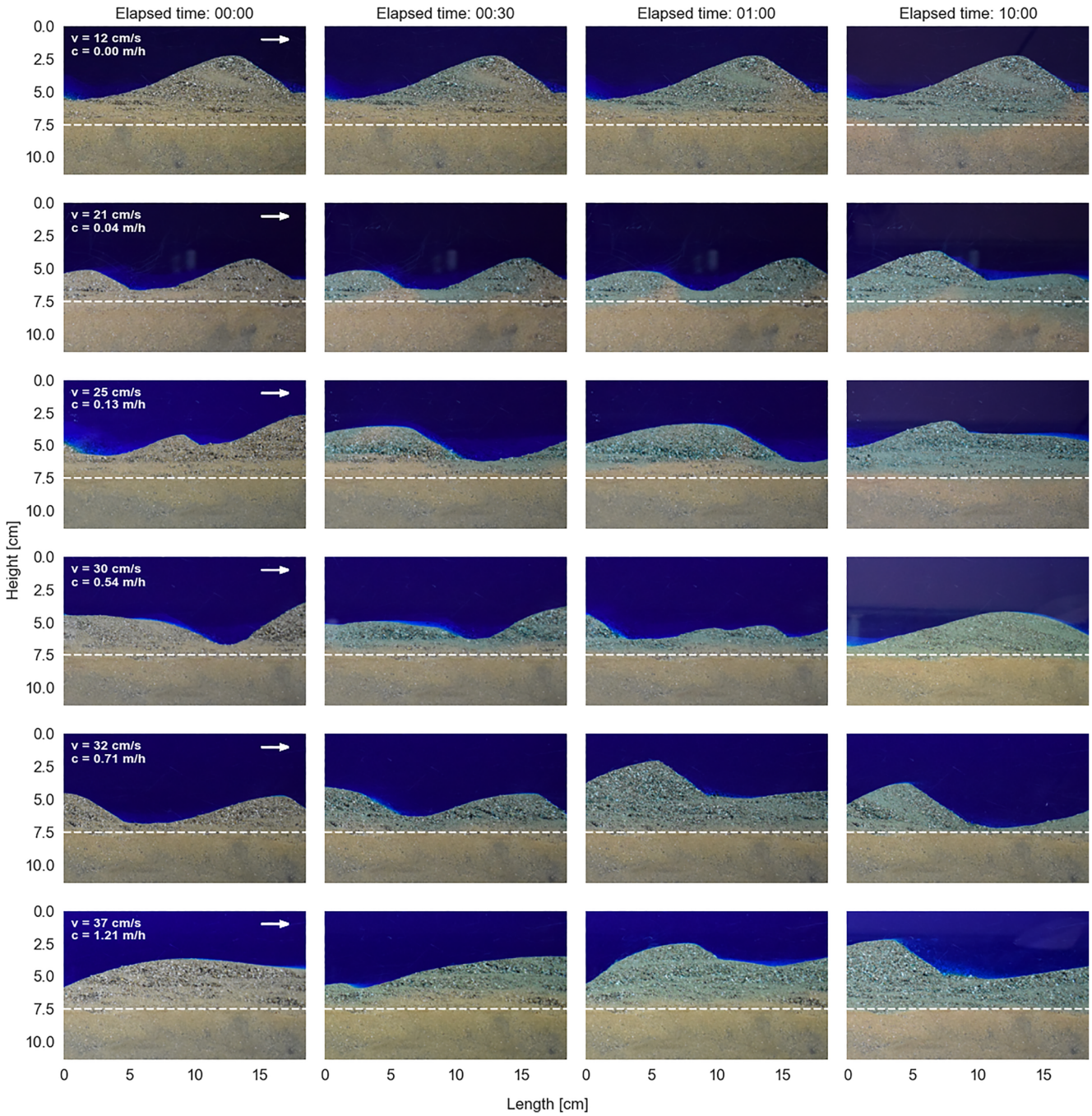

Figure 2. Time-lapse images of the dye-tracer experiments under six different streamwater velocities and bedform celerities. The blue-dyed areas within the streambed indicate where the streamwater is flowing within the sediment. Elapsed time is reported in the format: Hours:Minutes. The dashed horizontal line indicates the approximate location of the deepest scour depth.

the blue-colored area showed a crescent-shaped lower boundary that extended into the non-moving fraction of the streambed, while dye-free upwelling pore water was observed at the lee side of the bedform. This upwelling water with its distinct concentration pattern is commonly referred to as a "chimney" (Ahmerkamp et al., 2017; Huettel & Gust, 1992; Kessler et al., 2013). The chimney shrank and became blurred even at slow celerity (c = 0.04 m h^{-1}). Intermediate celerities (c = 0.04 and 0.13 m h^{-1}) show indications of a crescent-shaped HZ with a blurred chimney with patches of clear and dyed pore water that seem to be transported with the bedform. The faster the sediment moves, the more the HZ loses its crescent-shaped lower boundary, becomes flat, and the

chimneys disappear (c = 0.13–1.21 m h^{-1}). Within the fast-moving streambed, the dye does not reach into the non-moving fraction of the streambed (c = 0.13–1.21 m h^{-1}).

3.3. Distributions of O_2, CO_2, and pH Under Different Bedform Celerities

3.3.1. Spatial Distribution

The oxygen distribution in Figure 3 resembled the shape of the HZ as shown in the dye tracer experiments (Figure 2). The stationary bedform revealed a crescent-shaped oxygen distribution with a pronounced anoxic chimney (Figure 3, c = 0 m h^{-1}). The chimney became smaller and blurred, and disappeared with increasing bedform celerity. Oxygen concentrations decreased with sediment depth under all streamwater velocities, eventually reaching anoxic conditions. The interface between oxic and anoxic zones became sharper as celerity increased. High celerities (0.71 and 1.21 m h^{-1}) resulted in one fully mixed compartment of upper bed and the streamwater.

CO_2 concentrations were lower in the streamwater as compared to pore water concentrations under all flow conditions. CO_2 concentrations in the pore water increased by approximately one order of magnitude from the streamwater sediment interface to the lower section of the optode, a depth of approximately 8 cm. The distributions of CO_2 in the bed generally followed the shape of the HZ and O_2 concentrations (Figures 2 and 3, respectively). For example, a crescent-shaped distribution and pronounced chimney of high CO_2 concentration were observed in the stationary sediment, and flattened distributions with a relatively well-mixed moving fraction were observed under faster celerities (c = 0.54, 0.71, and 1.21 m h^{-1}). As celerity increased, the concentrations in the moving fraction approached those in the streamwater. Increasing celerities also led to a clearer interface between the well-mixed moving fraction and the non-moving fraction.

pH values ranged from ∼8.3 in the streamwater to a pH of ∼6.5 at the lower right end of the optode in the non-moving fraction. The pH in the moving fraction of the bed was slightly lower than the water under stationary (c = 0 m h^{-1}) and slow-moving conditions (c = 0.04 m h^{-1}). At higher celerities, there was no substantial difference between the moving fraction of the bed and the streamwater. The pH in the non-moving fraction of the bed was always substantially lower than in the moving fraction of the bed. The calculated DIC concentrations ranged from ∼1,600 to ∼2,050 µmol L^{-1} in the first experimental run and from ∼2,045 to ∼2,050 µmol L^{-1} in the last experimental run with a distribution equal to that of CO_2 (Figure S6 in Supporting Information S1).

3.3.2. Temporal Variability of O_2 and CO_2

The temporal dynamics of CO_2 and O_2 were measured during bedform movement over a period of 3–6 hr with intervals chosen depending on the celerity (Figure 4 and Figures S9 and S10 in Supporting Information S1). The spatial patterns and dynamics of the bed can be viewed as time-lapse images in the Supporting Information (Movies S1–S12 and Figure S8 in Supporting Information S1). No temporal dynamics were observed for either O_2 or CO_2 under stationary conditions. Maximum temporal variability was observed as soon as the bed started to move (c = 0.04 m h^{-1} in Figure 4, Figures S9 and S10 in Supporting Information S1). Movies from the same celerities showed chimneys of anoxic pore water moving with the bedforms, vanishing, and reforming (Movies S2 and S8). However, chimneys of higher CO_2 concentrations were not clearly visible. The variability of profiles was reduced with increasing celerity but still remained high as compared to stationary conditions. Time-lapse movies of faster celerities showed no chimneys and a more homogenized moving fraction. However, even under high celerities, the moving fraction often showed elevated CO_2 and lower O_2 concentrations compared to the streamwater.

3.4. O_2 Consumption and CO_2 Production

The oxic area, mean oxygen concentrations, and oxygen consumption rates increased with celerity (Figures 5a–5c). The consumption rates were lowest in stationary sediments and increased abruptly as soon as the bedform started to move. Further increase was linear (Figure 5c). The variability of oxygen consumption rates generally increased with celerity.

DIC production rates were lowest in the stationary streambed, increased abruptly as the sediment started to move, with a slight increase with increasing celerities (Figure 5e). These trends were considerably different from O_2 consumption rates. This discrepancy is mirrored in calculated RQs that are decreasing with increasing celerity

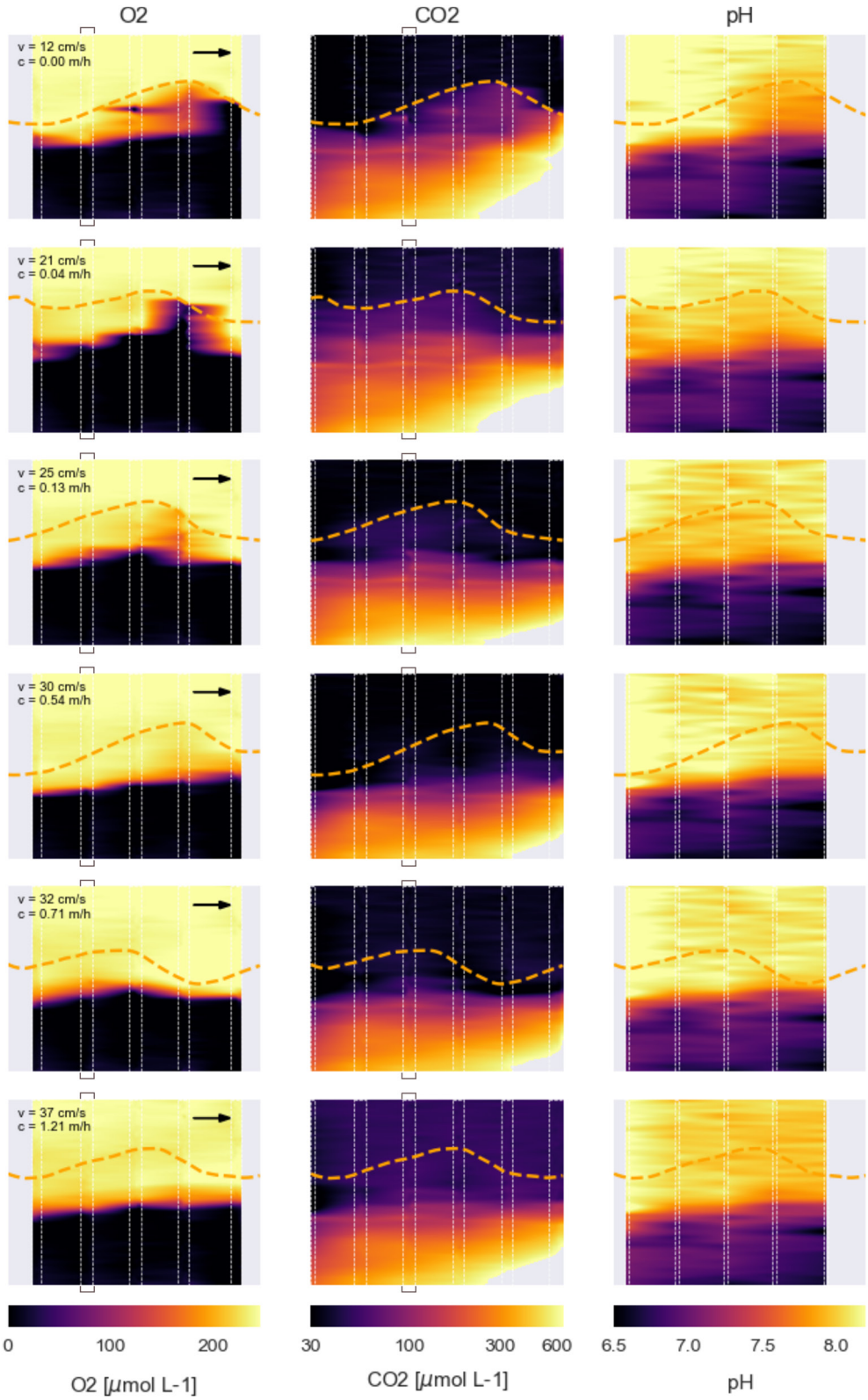
O2
CO2
pH
v = 12 cm/s
c = 0.00 m/h
v = 21 cm/s
c = 0.04 m/h
v = 25 cm/s
c = 0.13 m/h
v = 30 cm/s
c = 0.54 m/h
v = 32 cm/s
c = 0.71 m/h
v = 37 cm/s
c = 1.21 m/h
0
100
200
O2 [µmol L-1]
30
100
300
600
CO2 [µmol L-1]
6.5
7.0
7.5
8.0
pH

Figure 3.

(Figure 5f). Finally, the variability in the rates of DIC was larger than that of oxygen consumption rates. Because CO_2 and DIC production were similar, we will refer only to CO_2 in the remaining text (Figure S12 in Supporting Information S1).

CO_2 evasion had a positive correlation with celerity and velocity (Spearman Correlation Coefficient $R^2_{Sp} = 0.9$), as well as with CO_2 concentration in the streamwater ($R^2_{Sp} = 0.78$) (Figure S11 in Supporting Information S1). The correlation between CO_2 evasion and DIC production rates in the sediment was lower than the O_2 production rates ($R^2_{Sp} = 0.3$ and 0.53, respectively).

4. Discussion

This study combined measurements of O_2 and CO_2 concentrations in the stream and pore water of stationary and moving bedforms to explore the effect of celerity on the dynamics of O_2 consumption and CO_2 production (respiration) in the streambed. Most studies on microbial respiration in stream sediments focus on the reactant's side of the aerobic respiration reaction by attempting to quantify the oxygen consumed. Oxygen is relatively easy to measure given the vast amount and accuracy of oxygen sensors on the market (Bernhardt et al., 2018). Measuring CO_2 in addition to O_2 allows a more direct quantification of the fate of carbon in the form of CO_2 production, its fate in the streambed, and emission to the atmosphere. Recent advances in planar optode techniques provide new possibilities for visualizing the influence of moving bedforms on microbial respiration at the sediment-water interface (Santner et al., 2015). To the best of our knowledge, the present study is the first one using CO_2 optodes in moving bedforms and thus sheds new light on the dynamics of biogeochemical processes in the HZ.

4.1. Spatial and Temporal Distribution of O_2 and CO_2 in a Moving and Non-Moving Streambed

The spatial distributions of O_2 and CO_2 concentrations in the moving and non-moving fraction of the bed were strongly influenced by bedform shape and celerity, which is aligned with the first part of our hypothesis. In general, CO_2 concentrations were higher in the moving fraction as compared to the water column in stationary and slow-moving streambeds ($c \leq 0.13$ m h^{-1}). This suggests that CO_2 production exceeded the rate of transport. Advective pumping explains well the crescent-shaped HZ and upwelling anoxic pore water (chimneys) originating from deeper sediments that were moving with the moving sediment under low celerities. This was shown in previous flume studies for oxygen (Galloway et al., 2019; Kaufman et al., 2017; Precht et al., 2004), modeling studies for oxygen and dissolved nitrogen-containing compounds (Ahmerkamp et al., 2015; Kessler et al., 2015; Zheng et al., 2019), and for N_2O concentrations (Jiang et al., 2022). Upwelling water also contained high CO_2 concentrations stemming from production in the HZ and from CO_2 storage in deeper sediments (Figure 3). The chimney of upwelling water was less pronounced for CO_2 as compared to O_2, probably due to a lower resolution of CO_2 concentration as compared to those of O_2.

The transition from the low-celerity concentration patterns to the high-celerity ones was gradual. The crescent shape and chimney were more smeared as celerity increased ($c = 0.13$ m h^{-1}, Figure 3). Further increase in celerity (>0.54 m h^{-1}) caused rapid mixing of the moving fraction of the bed and resulted in complete disappearance of the chimney as also observed in other studies (Jiang et al., 2022; Kessler et al., 2015; Wolke et al., 2019). Under high celerities, solutes were unable to penetrate deeper into the streambed, because of flattened HEF flowpaths and by the increase in the extent of pore water that released back into the stream due to bed movement (turnover process) (Figures 2 and 3; Ahmerkamp et al., 2015). Fast bed movement ultimately isolated the non-moving from the moving fraction and, hence, reduced the supply of CO_2 from deeper sediments toward the surface and the delivery of O_2 from the stream to deeper sediments (redox seal) (Ahmerkamp et al., 2015; Bottacin-Busolin & Marion, 2010).

The isolation between the moving and non-moving fraction of the bed prevented the efficient release of CO_2 from deep storage zones toward the streamwater and the atmosphere (Jiang et al., 2022). The increasing CO_2 concentrations with depth in the non-moving fraction of the bed can be explained by diffusion of CO_2 from the

Figure 3. Distributions of O_2, CO_2, and pH within bedforms of similar shape under six streamwater velocities and bedform celerities. Orange dashed lines delineate the streamwater-sediment interface. Columns show distributions of different solutes: O_2 (left; O_2 air saturation = 246 μmol L^{-1}), CO_2 (middle; range: 30–644 μmol L^{-1}; logarithmic scale), and pH (right). Gray areas in the lower right corner of CO_2 images indicate that concentrations exceeded the calibration range (0–644 μmol L^{-1}). White dashed lines indicate optode stripes for which measured data exists, while the other data originate from grid interpolation. Square brackets indicate optode stripes used to show vertical profiles in Figure 4.

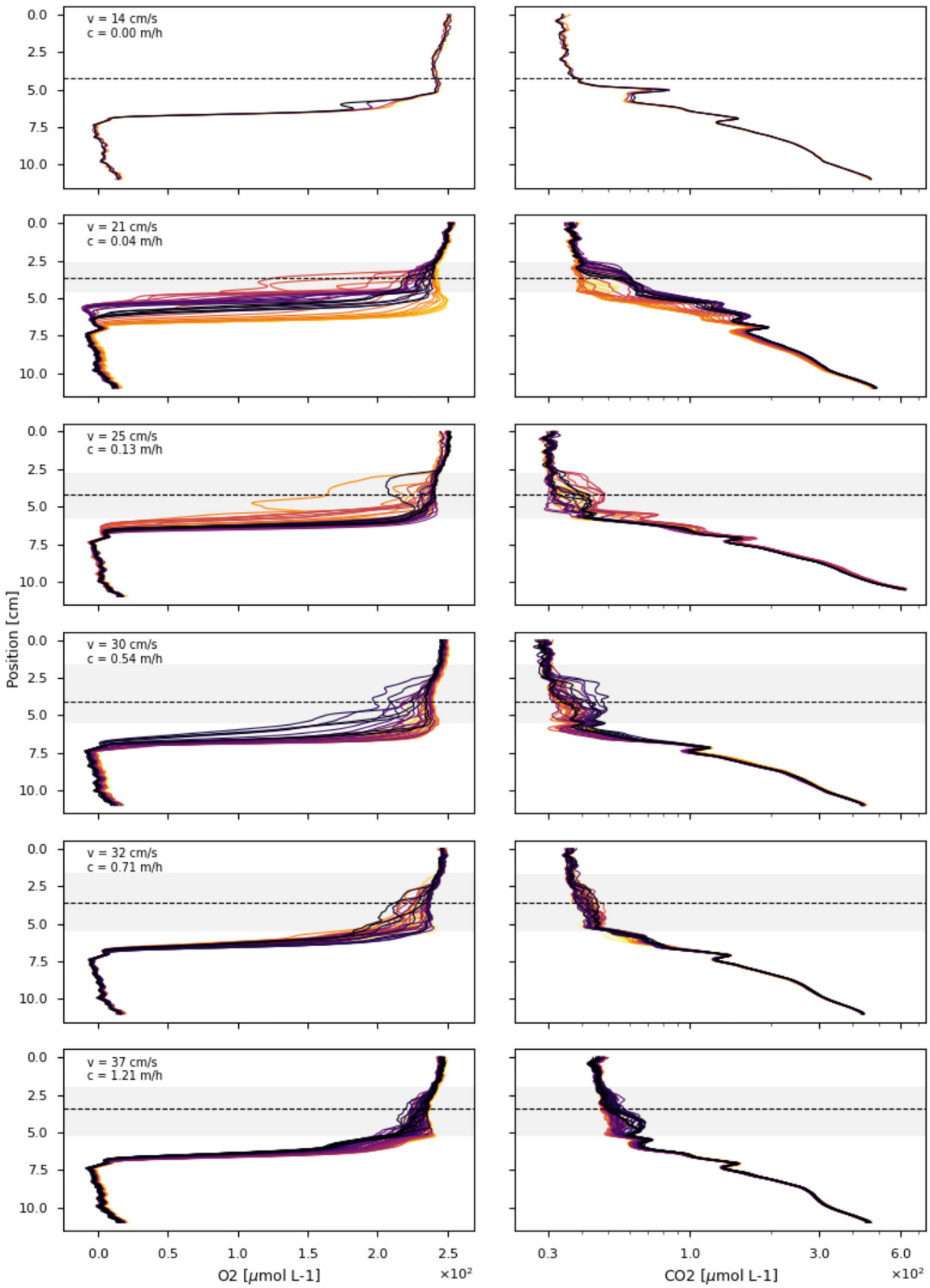

Figure 4. Evolution in time of O_2 (O_2 air saturation = 246 µmol L^{-1}) and CO_2 (range: 30–644 µmol L^{-1}; logarithmic scale) profiles that were measured for optode stripes indicated by square brackets in Figure 3. Colored lines show profiles taken during 3–6 hr of measurements. Color gradients from yellow (initial) to black (final) indicate the relative time elapsed. The dashed horizontal line and gray area indicate the mean location and the extent of the streamwater-sediment interface, respectively.

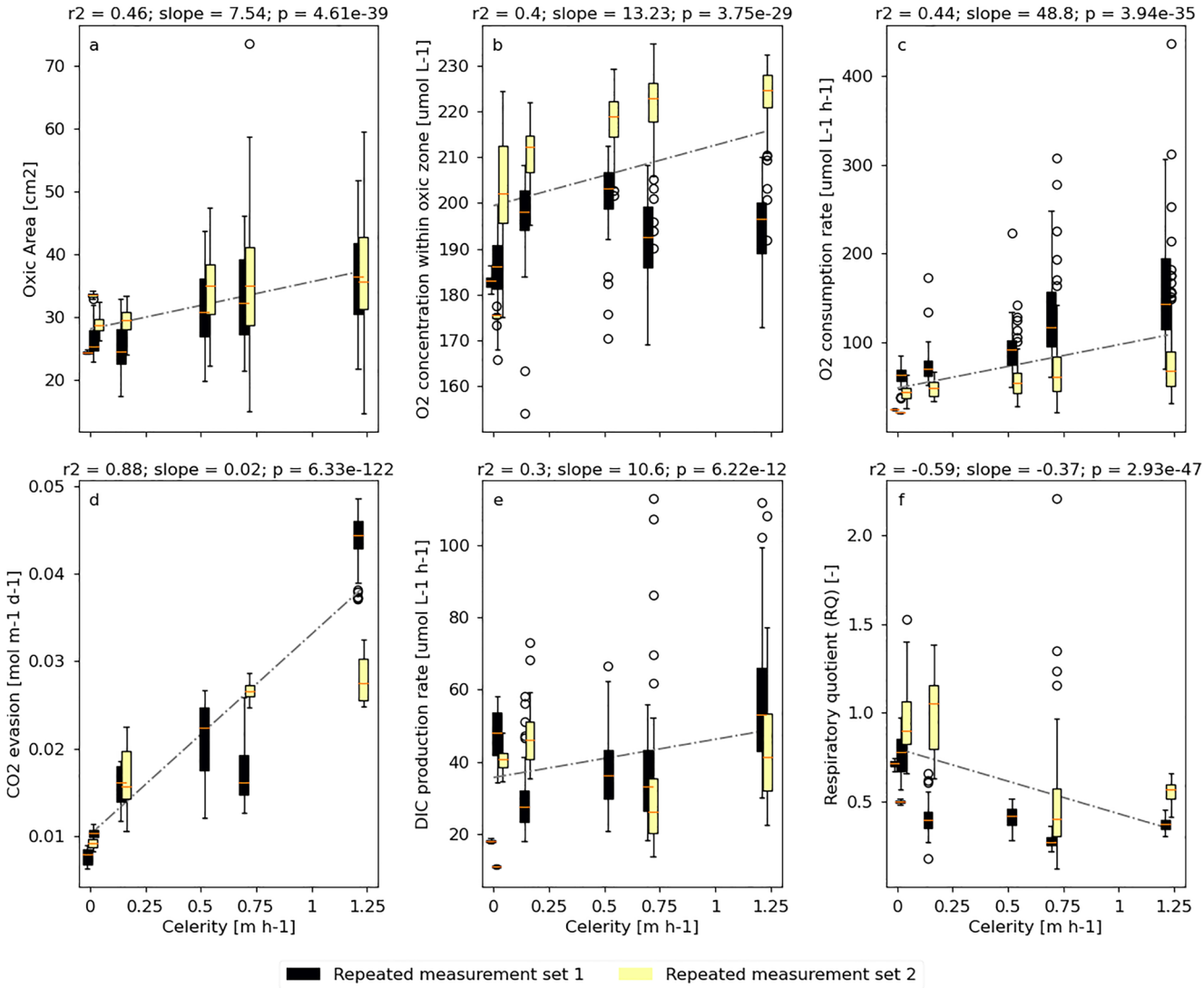

Figure 5. Relationship between bedform celerity and oxic area size within the sediment (a), mean O_2 concentration within the oxic area (b), oxygen consumption rates (c), CO_2 evasion (d), dissolved inorganic carbon (DIC) production rates (e), and respiratory quotient (f). Colors refer to two independent sets of experimental runs. Gray dashed lines show linear regression of the entire data set.

deeper sediments toward the moving fraction and the streamwater. Diffusion can release relatively small fractions of the stored CO_2. In addition, advective flow paths in stationary beds reach into deeper sediments and enhance the flushing of CO_2 toward the surface. The advective flow paths in combination with dispersion contribute to the increasing CO_2 concentration pattern with depth. Similar trends in storage and exchange of dissolved gas (N_2O) were also discussed in a recent modeling study by Jiang et al. (2022). We postulate that the accumulation of CO_2 in the deeper bed originated from variable sources. The first possible source is downwelling flow paths from the inlet zone of the flume, which transported CO_2 downstream by lateral pore water flow (underflow) induced by stream gradients of sloped streambeds (Laattoe et al., 2014; Sophocleous, 2002; Zhou & Endreny, 2013). Dispersion of the underflow potentially also contributed to the vertical concentration pattern observed in the non-moving fraction of the streambed. Second, CO_2 could have been formed by aerobic microbes in the initial phase of the experiment when the sediment still contained oxygen. Significant amounts of CO_2 might have been formed and stored in the deeper sediment. Another explanation may be that anaerobic processes in the anoxic areas of the streambed could have contributed to the CO_2 load. However, a systematic evaluation of the different processes was not conducted.

The temporal variability of CO_2 and O_2 concentrations was higher in the moving bed as compared to stationary sediments. Flow paths and biomass distribution in stationary bedforms are relatively constant under the time scales of the experimental runs, that is, few hours; thus, no variability was observed in the concentrations shown as 2-D distribution (Movies S1–S7) and 1-D profiles (Figure 4). When considering stationary streambeds only, temporal variability of distributions might be disregarded. The notion that pore water flow is slow compared to streamwater flow and temporal variability is therefore minor is not correct for moving streambeds. During bed movement, bedform shape and pore water flow paths in moving sediments change, which alters the measured concentration at a fixed place in the sediment. The highest variability was observed in slow-moving streambeds (c = 0.04 m h^{-1}; Figure 4, Movies S2 and S8). Here, crescent-shaped distributions cause high variability of concentrations in the moving fraction of the streambed, which is continuously altered due to bedform movement. Even if *Da* numbers are relatively low under higher compared to lower celerities, a *Da* above 1 still indicates a highly reactive system that outscores transport processes. The observed temporal variability can be linked to the variability of calculated O_2 consumption and production rates of CO_2 and DIC (Figures 5c–5e).

4.2. CO_2 Production Rates and Biogeochemical Activity in Moving Streambeds

O_2 consumption and CO_2 production rates increased abruptly when the bed started moving, and a more moderate increase in rates was observed with increasing celerity (Figure 5). This observation contradicts our second hypothesis which suggested a decreasing relationship between celerity and respiration. A possible explanation for the increase in respiration rates with celerity is the increased O_2 supply to the subsurface by the increasing HEF (Table 1 and Figure S7 in Supporting Information S1).

RQs vary with the type of respiratory substrate in a range between 0.8 and 1.2 (Bott, 2007; Williams & del Giorgio, 2005). The RQs in stationary beds and at lowest celerities are well within this expected range. However, relatively low mean RQs were observed at high celerities (Figure 5f). A possible explanation for the low RQ may stem from the relatively long response times needed for the CO_2 optode measurement (t_{90} < 3 min) relative to that of the oxygen (<30 min). At higher celerity ($c \geq$ 50 cm h^{-1}), the movement of the bedform may outpace the slowly responding CO_2-optodes, which then measure a biased signal resulting from averaging conditions in the moving fraction of the sediment and streamwater. As the optode signal is only partially capturing the moving bedform, the accuracy of the CO_2 measurements decreases. In addition, CO_2 production rates are calculated based on the oxic area of the sediment only, which might exclude produced CO_2 at the fringes of the oxic area and CO_2 transported away from the assessed area by pore water flow. From an ecological standpoint, the RQ is dependent on the quality and bioavailability of dissolved organic matter (DOM) (Singer et al., 2011). DOM is a complex mixture of compounds from various sources of varying bioavailability that can include easily degradable, labile over semi-labile to recalcitrant molecules (Kaplan & Newbold, 2003; Singer et al., 2011). It is plausible that the observed decreasing RQ with celerity may be explained by the selective use of carbon sources of different quality and bioavailability under various celerities. However, direct measurements of the DOM quality were not done during the experiments.

Previous studies reported different trends of O_2 consumption with increasing celerities. For instance, Ahmerkamp et al. (2017) and Wolke et al. (2019) observed a reduction in O_2 consumption with increasing celerities, while an increase in aerobic biogeochemical activity with celerity was observed by two modeling studies on aerobic respiration (Kessler et al., 2015) and nitrification (Kessler et al., 2015; Zheng et al., 2019). These diverging results are not surprising because volumetric reaction rates depend on the interplay between hydrological conditions, biomass abundance, and local reaction rates, which are challenging to determine under moving bed conditions. The effect of celerity on reaction rates in the sediment is probably more complex than considered until now, because of the incomplete information on microbial biomass and how it responds to sediment movement.

Conflicting trends between celerity and reaction rates in experimental studies may originate from differences in experimental setting and reactivity of the investigated sediments. For instance, Ahmerkamp et al. (2017) observed an overall decreasing trend of O_2 consumption rates with increasing celerity. They compared stationary and slowly moving bedforms in a marine pristine environment and reported, in accordance with our results, lower Da-numbers in moving compared to stationary streambeds. However, their Da-numbers approached or were smaller than 1 in moving streambeds, indicating that pore water exchange was faster than O_2 consumption, leading to an overall decrease in consumption rates. This is not surprising since the organic matter content of the marine sediment was relatively low (0.03%–0.37%) and the exchange flow was probably smaller than in our study

due to the lower water velocity (5–22 vs. 12–37 cm s^{-1}). The Da-numbers found in the present study were greater than 1 under all celerities, suggesting that biogeochemical activity was more dominant than pore water velocity.

Comparing the results of biogeochemical processes under moving streambeds is challenging. For instance, different approaches to determine HEF in Wolke et al. (2019) and the present study may explain the discrepant trend of oxygen consumption rates with celerity. Furthermore, some studies relied on batch experiments with samples taken from moving and stationary streambeds (Ahmerkamp et al., 2017). Others used agitated microcosms where they compared stationary non-disturbed sediments with periodic (Zlatanović et al., 2017) or continuous agitations (Scheidweiler et al., 2021). Batch experiments can capture some of the physical effects of the sediment movement (e.g., mechanical stress) but cannot capture accurately the transport processes between the stream and the HZ. Ultimately, the effect of moving bedforms on biogeochemical processes should be preferably studied in the field or in a realistic system where natural sediments are used and bedforms are moving in a controlled way.

In summary, CO_2 evasion showed a positive relationship with stream velocity, bedform celerity, and CO_2 concentration in the surface water. This suggests that streamwater velocity is an important factor to consider while evaluating metabolism in streams with fine sediments. The correlation between evasion and DIC production rates in the sediment was relatively low as compared to that of O_2 consumption rates. A possible explanation for this is the relatively low production of CO_2 compared to the amount of O_2 consumed as illustrated by the reduction in RQs with an increase in celerity, which is probably due to measurement inaccuracies under high celerities.

4.3. Field Implications

Understanding the dynamics of CO_2 production and distribution during bedform motion is crucial because sandy streambeds are found all over the world and predominantly encountered in lowland topography (Buffington & Montgomery, 2022). The contribution of sediment respiration to the in-stream CO_2 load was found to be highest in lowland streams where soil-water inputs are less important as compared to headwaters (Lauerwald et al., 2015). The present study showed that the most dramatic increase in CO_2 production rates occurred when the bed shifts between stationary and slowly moving bedforms. This suggests that bed movement should be measured and taken into account already under base flow conditions and not only during high flow events. It is also estimated that the impact of moving bedforms is especially high in nutrient-rich urban and agriculturally influenced rivers. In these, potentially high influx of nutrient-rich and of labile DOC-rich streamwater into the HZ may strongly fortify the CO_2 production in the streambed (Baker et al., 1999; Comer-Warner et al., 2018; Romeijn et al., 2019).

The results also showed that celerity of bedforms influences the CO_2 transient storage in the streambed and the exchange between moving and non-moving fractions. We assume that the relationship between bedform movement and transient storage is abundant in the field, but to the best of our knowledge, there is no study that investigated CO_2 distribution in the streambed with respect to sediment movement. In accordance with our results, CO_2 concentrations in the streambed are generally elevated with respect to streamwater concentrations (Hlaváčová et al., 2005; Peter et al., 2014; Schindler & Krabbenhoft, 1998). This suggests that sediments are temporary storage zones of CO_2, which can slowly diffuse toward the streamwater along concentration gradients (Peter et al., 2014), can be transported by advection in upwelling zones (Hlaváčová et al., 2005), or can be abruptly released when deep bed scour occurs during flood events. Under gaining flow conditions, we do not expect to see storage of CO_2 due to constant upwelling flow paths. On the other hand, losing flow conditions can contribute CO_2 to storage zones in the deep sediments and groundwater (Peter et al., 2014).

CO_2 evasion from inland waters has been extensively studied (Stanley et al., 2016). However, most studies have focused on estimating the amount of evasion and do not report other measurements that enable to pinpoint the underlying processes. Understanding and consideration of those processes are essential to be able to upscale and predict in-stream CO_2 and evasion on local, catchment, and global scales. This study highlights the importance of linking streamwater velocity and bedform movement as physical drivers for sedimentary CO_2 production and storage. It stresses the importance of including bedform movement into biogeochemical studies in general, and in studies on CO_2 evasion in particular. Our study also demonstrates that specific sampling efforts are required to fully capture the transport and reaction processes in sandy streams. These efforts should include the evaluation of bedform celerity and measurements of the spatial and temporal distribution of CO_2 in the bed. Hydrological parameters, including the assessment of the HEF and the exchange flux and direction between surface and groundwater, are also essential for quantification of reaction rates and CO_2 evasion.

5. Conclusions

This study illustrated that bedform celerity has a substantial impact on the spatial and temporal distributions of CO_2, as well as on CO_2 production rates. The distribution of O_2 and CO_2 resembled the shape of the flow paths within the HZ. Advection was dominant under all celerities, but increasing contribution of turnover to the overall exchange occurred as celerity increased. Turnover caused flattening of the HZ bottom boundary, which ultimately resulted in an HZ shape resembling the shape of the moving fraction of the bed. High celerities caused isolation of the non-moving fractions of the bed leading to substantial storage of CO_2 in deeper sections of the bed. HEF and CO_2 production rates increased first rapidly and then more gradually with increasing celerity. This suggests that, although the system was reaction-dominated ($Da > 1$), HEF played an important role in biogeochemical processes in moving bedforms. Moreover, moving bedforms show an unexpected impact on transient storage and exchange of CO_2 between the streambed and the streamwater, which requires more attention in field measurements and should be incorporated into estimations of CO_2 evasion from streams.

Conflict of Interest

The authors declare no conflicts of interest relevant to this study.

Data Availability Statement

All data used in this study are available via Zenodo: https://doi.org/10.5281/zenodo.7674577.

Acknowledgments
This research was funded by the European Union's Horizon 2020 Research and Innovation Program under the Marie Sklodowska-Curie Grant agreement no. 765553 (EuroFlow) and the Israel Science Foundation, Grant 682/17. Further funding was supplied by the German Research Foundation (DFG) as part of the research project "Urban Water Interfaces (UWI)" (GRK 2032), and by the German Federal Ministry of Education and Research (BMBF) and the Israeli Ministry of Science, Technology and Space (MOST) in the framework of the German-Israeli Cooperation in Water Technology Research as part of the Young Scientist Exchange Program (YSEP136). The authors also thank Silvia Gobrecht, Amir Maimon, and Noam Yogev for laboratory assistance, and Anna Lena Kronsbein, Birgit Maria Müller, and Karsten Berg for fruitful discussions and additional support. Open Access funding enabled and organized by Projekt DEAL.

References

Ahmerkamp, S., Winter, C., Janssen, F., Kuypers, M. M. M., & Holtappels, M. (2015). The impact of bedform migration on benthic oxygen fluxes: Bedform migration and benthic fluxes. *Journal of Geophysical Research: Biogeosciences*, *120*(11), 2229–2242. https://doi.org/10.1002/2015JG003106

Ahmerkamp, S., Winter, C., Krämer, K., Beer, D. d., Janssen, F., Friedrich, J., et al. (2017). Regulation of benthic oxygen fluxes in permeable sediments of the coastal ocean: Regulation of benthic oxygen fluxes. *Limnology & Oceanography*, *62*(5), 1935–1954. https://doi.org/10.1002/lno.10544

Amiotte-Suchet, P., Aubert, D., Probst, J. L., Gauthier-Lafaye, F., Probst, A., Andreux, F., & Viville, D. (1999). delta13C pattern of dissolved inorganic carbon in a small granitic catchment: The Strengbach case study (Vosges mountains, France). *Chemical Geology*, *159*(1), 129–145. https://doi.org/10.1016/S0009-2541(99)00037-6

Arnon, S., Avni, N., & Gafny, S. (2015). Nutrient uptake and macroinvertebrate community structure in a highly regulated Mediterranean stream receiving treated wastewater. *Aquatic Sciences*, *77*(4), 623–637. https://doi.org/10.1007/s00027-015-0407-6

Baker, M. A., Dahm, C. N., & Valett, H. M. (1999). Acetate retention and metabolism in the hyporheic zone of a mountain stream. *Limnology & Oceanography*, *44*(6), 1530–1539. https://doi.org/10.4319/lo.1999.44.6.1530

Bastviken, D., Sundgren, I., Natchimuthu, S., Reyier, H., & Gålfalk, M. (2015). Technical Note: Cost-efficient approaches to measure carbon dioxide (CO_2) fluxes and concentrations in terrestrial and aquatic environments using mini loggers. *Biogeosciences*, *12*(12), 3849–3859. https://doi.org/10.5194/bg-12-3849-2015

Battin, T. J., Luyssaert, S., Kaplan, L. A., Aufdenkampe, A. K., Richter, A., & Tranvik, L. J. (2009). The boundless carbon cycle. *Nature Geoscience*, *2*(9), 598–600. https://doi.org/10.1038/ngeo618

Bernhardt, E. S., Heffernan, J. B., Grimm, N. B., Stanley, E. H., Harvey, J. W., Arroita, M., et al. (2018). The metabolic regimes of flowing waters. *Limnology & Oceanography*, *63*(S1), S99–S118. https://doi.org/10.1002/lno.10726

Boano, F., Harvey, J. W., Marion, A., Packman, A. I., Revelli, R., Ridolfi, L., & Wörman, A. (2014). Hyporheic flow and transport processes: Mechanisms, models, and biogeochemical implications. *Reviews of Geophysics*, *52*(4), 603–679. https://doi.org/10.1002/2012RG000417

Bott, T. L. (2007). Primary productivity and community respiration. In F. R. Hauer & G. A. Lamberti (Eds.), *Methods in stream ecology* (2nd ed., pp. 663–690). Academic Press.

Bottacin-Busolin, A., & Marion, A. (2010). Combined role of advective pumping and mechanical dispersion on time scales of bed form–induced hyporheic exchange. *Water Resources Research*, *46*(8), W08518. https://doi.org/10.1029/2009WR008892

Bradski, G. (2000). The OpenCV library. *Dr. Dobb's Journal of Software Tools*(120), 122–125.

Brodersen, K. E., Koren, K., Moßhammer, M., Ralph, P. J., Kühl, M., & Santner, J. (2017). Seagrass-mediated phosphorus and iron solubilization in tropical sediments. *Environmental Science & Technology*, *51*(24), 14155–14163. https://doi.org/10.1021/acs.est.7b03878

Buffington, J. M., & Montgomery, D. R. (2022). 6.51 – Geomorphic classification of rivers: An updated review. In J. J. F. Shroder (Ed.), *Treatise on geomorphology* (2nd ed., pp. 1143–1190). Academic Press.

Cole, J. J., Prairie, Y. T., Caraco, N. F., McDowell, W. H., Tranvik, L. J., Striegl, R. G., et al. (2007). Plumbing the global carbon cycle: Integrating inland waters into the terrestrial carbon budget. *Ecosystems*, *10*(1), 172–185. https://doi.org/10.1007/s10021-006-9013-8

Comer-Warner, S. A., Romeijn, P., Gooddy, D. C., Ullah, S., Kettridge, N., Marchant, B., et al. (2018). Thermal sensitivity of CO_2 and CH_4 emissions varies with streambed sediment properties. *Nature Communications*, *9*(1), 2803. https://doi.org/10.1038/s41467-018-04756-x

Crawford, J. T., & Stanley, E. H. (2016). Controls on methane concentrations and fluxes in streams draining human-dominated landscapes. *Ecological Applications*, *26*(5), 1581–1591. https://doi.org/10.1890/15-1330

Dallmann, J., Phillips, C. B., Teitelbaum, Y., Sund, N., Schumer, R., Arnon, S., & Packman, A. I. (2020). Impacts of suspended clay particle deposition on sand-bed morphodynamics. *Water Resources Research*, *56*(8), e2019WR027010. https://doi.org/10.1029/2019WR027010

De Falco, N., Boano, F., & Arnon, S. (2016). Biodegradation of labile dissolved organic carbon under losing and gaining streamflow conditions simulated in a laboratory flume. *Limnology & Oceanography*, *61*(5), 1839–1852. https://doi.org/10.1002/lno.10344

De Falco, N., Boano, F., Bogler, A., Bar-Zeev, E., & Arnon, S. (2018). Influence of stream-subsurface exchange flux and bacterial biofilms on oxygen consumption under nutrient-rich conditions. *Journal of Geophysical Research: Biogeosciences*, *123*(7), 2021–2034. https://doi.org/10.1029/2017JG004372

Devlin, J. F. (2016). HydrogeoSieveXL: An excel-based tool to estimate hydraulic conductivity from grain-size analysis. *Hydrogeology*, *23*(4), 837–844. https://doi.org/10.1007/s10040-015-1255-0

Elliott, A. H., & Brooks, N. H. (1997a). Transfer of nonsorbing solutes to a streambed with bed forms: Laboratory experiments. *Water Resources Research*, *33*(1), 137–151. https://doi.org/10.1029/96WR02783

Elliott, A. H., & Brooks, N. H. (1997b). Transfer of nonsorbing solutes to a streambed with bed forms: Theory. *Water Resources Research*, *33*(1), 123–136. https://doi.org/10.1029/96WR02784

Fellows, C., Valett, H., & Dahm, C. (2001). Whole-stream metabolism in two montane streams: Contribution of the hyporheic zone. *Limnology & Oceanography*, *46*(3), 523–531. https://doi.org/10.4319/lo.2001.46.3.0523

Finlay, J. C. (2003). Controls of streamwater dissolved inorganic carbon dynamics in a forested watershed. *Biogeochemistry*, *62*(3), 231–252. https://doi.org/10.1023/A:1021183023963

Fox, A., Boano, F., & Arnon, S. (2014). Impact of losing and gaining streamflow conditions on hyporheic exchange fluxes induced by dune-shaped bed forms. *Water Resources Research*, *50*(3), 1895–1907. https://doi.org/10.1002/2013WR014668

Galloway, J., Fox, A., Lewandowski, J., & Arnon, S. (2019). The effect of unsteady streamflow and stream-groundwater interactions on oxygen consumption in a sandy streambed. *Scientific Reports*, *9*(1), 19735. https://doi.org/10.1038/s41598-019-56289-y

Ge, L., Tan, H., Chen, X., Rao, W., & Fan, M. (2021). Dissolved inorganic carbon isotopes of a typical alpine river on the Tibetan Plateau revealing carbon sources, wetland effect and river recharge. *Hydrological Processes*, *35*(10), e14402. https://doi.org/10.1002/hyp.14402

Gomez-Velez, J. D., & Harvey, J. W. (2014). A hydrogeomorphic river network model predicts where and why hyporheic exchange is important in large basins. *Geophysical Research Letters*, *41*(18), 6403–6412. https://doi.org/10.1002/2014GL061099

Gomez-Velez, J. D., Harvey, J. W., Cardenas, M. B., & Kiel, B. (2015). Denitrification in the Mississippi River network controlled by flow through river bedforms. *Nature Geoscience*, *8*(12), 941–945. https://doi.org/10.1038/ngeo2567

Gooseff, M. N. (2010). Defining hyporheic zones – Advancing our conceptual and operational definitions of where stream water and groundwater meet. *Geography Compass*, *4*(8), 945–955. https://doi.org/10.1111/j.1749-8198.2010.00364.x

Gu, C., Waldron, S., & Bass, A. M. (2021). Carbon dioxide, methane, and dissolved carbon dynamics in an urbanized river system. *Hydrological Processes*, *35*(9), e14360. https://doi.org/10.1002/hyp.14360

Harvey, J. W., Wagner, B. J., & Bencala, K. E. (1996). Evaluating the reliability of the stream tracer approach to characterize stream-subsurface water exchange. *Water Resources Research*, *32*(8), 2441–2451. https://doi.org/10.1029/96WR01268

Hlaváčová, E., Rulík, M., & Čáp, L. (2005). Anaerobic microbial metabolism in hyporheic sediment of a gravel bar in a small lowland stream. *River Research and Applications*, *21*(9), 1003–1011. https://doi.org/10.1002/rra.866

Hope, D., Palmer, S. M., Billett, M. F., & Dawson, J. J. C. (2004). Variations in dissolved CO_2 and CH_4 in a first-order stream and catchment: An investigation of soil–stream linkages. *Hydrological Processes*, *18*(17), 3255–3275. https://doi.org/10.1002/hyp.5657

Hotchkiss, E. R., Hall, R. O., Jr., Sponseller, R. A., Butman, D., Klaminder, J., Laudon, H., et al. (2015). Sources of and processes controlling CO_2 emissions change with the size of streams and rivers. *Nature Geoscience*, *8*(9), 696–699. https://doi.org/10.1038/ngeo2507

Huettel, M., & Gust, G. (1992). Solute release mechanisms from confined sediment cores in stirred benthic chambers and flume flows. *Marine Ecology Progress Series*, *82*(2), 187–197. https://doi.org/10.3354/meps082187

Humphreys, M. P., Lewis, E. R., Sharp, J. D., & Pierrot, D. (2022). PyCO2SYS v1.8: Marine carbonate system calculations in Python. *Geoscientific Model Development*, *15*(1), 15–43. https://doi.org/10.5194/gmd-15-15-2022

Humphreys, M. P., Sandborn, D. E., Gregor, L., Pierrot, D., van Heuven, S. M. A. C., Lewis, E. R., & Wallace, D. W. R. (2022). PyCO2SYS: Marine carbonate system calculations in Python. *Zenodo*. https://doi.org/10.5281/zenodo.3744275

Hutchinson, P. A., & Webster, I. T. (1998). Solute uptake in aquatic sediments due to current-obstacle interactions. *Journal of Environmental Engineering*, *124*(5), 419–426. https://doi.org/10.1061/(ASCE)0733-9372(1998)124:5(419)

Jiang, Q., Liu, D., Jin, G., Tang, H., Wei, Q., & Xu, J. (2022). N_2O dynamics in the hyporheic zone due to ripple migration. *Journal of Hydrology*, *610*, 127891. https://doi.org/10.1016/j.jhydrol.2022.127891

Jones, J. B., Jr., Stanley, E. H., & Mulholland, P. J. (2003). Long-term decline in carbon dioxide supersaturation in rivers across the contiguous United States. *Geophysical Research Letters*, *30*(10), 1495. https://doi.org/10.1029/2003GL017056

Kaplan, L. A., & Newbold, J. D. (2003). 4 – The role of monomers in stream ecosystem metabolism. In S. E. G. Findlay & R. L. Sinsabaugh (Eds.), *Aquatic ecosystems* (pp. 97–119). Academic Press. https://doi.org/10.1016/B978-012256371-3/50005-6

Kaufman, M. H., Cardenas, M. B., Buttles, J., Kessler, A. J., & Cook, P. L. M. (2017). Hyporheic hot moments: Dissolved oxygen dynamics in the hyporheic zone in response to surface flow perturbations. *Water Resources Research*, *53*(8), 6642–6662. https://doi.org/10.1002/2016WR020296

Kessler, A. J., Cardenas, M. B., & Cook, P. L. M. (2015). The negligible effect of bed form migration on denitrification in hyporheic zones of permeable sediments. *Journal of Geophysical Research: Biogeosciences*, *120*(3), 538–548. https://doi.org/10.1002/2014JG002852

Kessler, A. J., Glud, R. N., Cardenas, M. B., & Cook, P. L. M. (2013). Transport zonation limits coupled nitrification-denitrification in permeable sediments. *Environmental Science & Technology*, *47*(23), 13404–13411. https://doi.org/10.1021/es403318x

Laattoe, T., Werner, A. D., & Post, V. E. A. (2014). Spatial periodicity in bed form-scale solute and thermal transport models of the hyporheic zone. *Water Resources Research*, *50*(10), 7886–7899. https://doi.org/10.1002/2014WR015361

Lauerwald, R., Laruelle, G. G., Hartmann, J., Ciais, P., & Regnier, P. A. (2015). Spatial patterns in CO_2 evasion from the global river network. *Global Biogeochemical Cycles*, *29*(5), 534–554. https://doi.org/10.1002/2014GB004941

Lewandowski, J., Arnon, S., Banks, E., Batelaan, O., Betterle, A., Broecker, T., et al. (2019). Is the hyporheic zone relevant beyond the scientific community? *Water*, *11*(11), 2230. https://doi.org/10.3390/w11112230

Marx, A., Dusek, J., Jankovec, J., Sanda, M., Vogel, T., van Geldern, R., et al. (2017). A review of CO_2 and associated carbon dynamics in headwater streams: A global perspective. *Reviews of Geophysics*, *55*(2), 560–585. https://doi.org/10.1002/2016RG000547

Mueller, B. M., Schulz, H., & Lewandowski, J. (2022). Hyporheic zone and processes. In T. Mehner & K. Tockner (Eds.), *Encyclopedia of inland waters* (2nd ed., pp. 301–311). Elsevier.

Naegeli, M. W., & Uehlinger, U. (1997). Contribution of the hyporheic zone to ecosystem metabolism in a prealpine gravel-bed-river. *Journal of the North American Benthological Society*, *16*(4), 794–804. https://doi.org/10.2307/1468172

Oliver, R. L., & Merrick, C. J. (2006). Partitioning of river metabolism identifies phytoplankton as a major contributor in the regulated Murray River (Australia). *Freshwater Biology*, *51*(6), 1131–1148. https://doi.org/10.1111/j.1365-2427.2006.01562.x

Packman, A. I., & Brooks, N. H. (2001). Hyporheic exchange of solutes and colloids with moving bed forms. *Water Resources Research*, *37*(10), 2591–2605. https://doi.org/10.1029/2001WR000477

Parkhurst, D. L., & Appelo, C. (2013). *Description of input and examples for PHREEQC version 3: A computer program for speciation, batch-reaction, one-dimensional transport, and inverse geochemical calculations (USGS Numbered Series No. 6-A43)*. U.S. Geological Survey.
Pennington, R., Argerich, A., & Haggerty, R. (2018). Measurement of gas-exchange rate in streams by the oxygen–carbon method. *Freshwater Science*, *37*(2), 222–237. https://doi.org/10.1086/698018
Peter, H., Singer, G. A., Preiler, C., Chifflard, P., Steniczka, G., & Battin, T. J. (2014). Scales and drivers of temporal pCO2 dynamics in an Alpine stream. *Journal of Geophysical Research: Biogeosciences*, *119*(6), 1078–1091. https://doi.org/10.1002/2013JG002552
Precht, E., Franke, U., Polerecky, L., & Huettel, M. (2004). Oxygen dynamics in permeable sediments with wave-driven pore water exchange. *Limnology & Oceanography*, *49*(3), 693–705. https://doi.org/10.4319/lo.2004.49.3.0693
Rasilo, T., Hutchins, R. H. S., Ruiz-González, C., & del Giorgio, P. A. (2017). Transport and transformation of soil-derived CO_2, CH_4 and DOC sustain CO_2 supersaturation in small boreal streams. *Science of the Total Environment*, *579*, 902–912. https://doi.org/10.1016/j.scitotenv.2016.10.187
Raymond, P. A., Hartmann, J., Lauerwald, R., Sobek, S., McDonald, C., Hoover, M., et al. (2013). Global carbon dioxide emissions from inland waters. *Nature*, *503*(7476), 355–359. https://doi.org/10.1038/nature12760
Raymond, P. A., Zappa, C. J., Butman, D., Bott, T. L., Potter, J., Mulholland, P., et al. (2012). Scaling the gas transfer velocity and hydraulic geometry in streams and small rivers: Gas transfer velocity and hydraulic geometry. *Limnology and Oceanography: Fluids and Environments*, *2*(1), 41–53. https://doi.org/10.1215/21573689-1597669
Regnier, P., Friedlingstein, P., Ciais, P., Mackenzie, F. T., Gruber, N., Janssens, I. A., et al. (2013). Anthropogenic perturbation of the carbon fluxes from land to ocean. *Nature Geoscience*, *6*(8), 597–607. https://doi.org/10.1038/ngeo1830
Romeijn, P., Comer-Warner, S. A., Ullah, S., Hannah, D. M., & Krause, S. (2019). Streambed organic matter controls on carbon dioxide and methane emissions from streams. *Environmental Science & Technology*, *53*(5), 2364–2374. https://doi.org/10.1021/acs.est.8b04243
Rovelli, L., Olde, L., Heppell, C., Binley, A., Yvon-Durocher, G., Glud, R., & Trimmer, M. (2022). Contrasting biophysical controls on carbon dioxide and methane outgassing from streams. *Journal of Geophysical Research: Biogeosciences*, *127*(1), e2021JG006328. https://doi.org/10.1029/2021JG006328
Saccardi, B., & Winnick, M. (2021). Improving predictions of stream CO_2 concentrations and fluxes using a stream network model: A case study in the East River Watershed, CO, USA. *Global Biogeochemical Cycles*, *35*(12), e2021GB006972. https://doi.org/10.1029/2021GB006972
Santner, J., Larsen, M., Kreuzeder, A., & Glud, R. N. (2015). Two decades of chemical imaging of solutes in sediments and soils – A review. *Analytica Chimica Acta*, *878*, 9–42. https://doi.org/10.1016/j.aca.2015.02.006
Scheidweiler, D., Mendoza-Lera, C., Mutz, M., & Risse-Buhl, U. (2021). Overlooked implication of sediment transport at low flow: Migrating ripples modulate streambed phototrophic and heterotrophic microbial activity. *Water Resources Research*, *57*(3), e2020WR027988. https://doi.org/10.1029/2020WR027988
Schindler, J. E., & Krabbenhoft, D. P. (1998). The hyporheic zone as a source of dissolved organic carbon and carbon gases to a temperate forested stream. *Biogeochemistry*, *43*(2), 157–174. https://doi.org/10.1023/A:1006005311257
Singer, G., Besemer, K., Hochedlinger, G., Chlup, A., & Battin, T. (2011). Monomeric carbohydrate uptake and structure–function coupling in stream biofilms. *Aquatic Microbial Ecology*, *62*(1), 71–83. https://doi.org/10.3354/ame01454
Singh, H. (2019). *Practical machine learning and image processing: For facial recognition, object detection, and pattern recognition using Python*. Apress. https://doi.org/10.1007/978-1-4842-4149-3
Sophocleous, M. (2002). Interactions between groundwater and surface water: The state of the science. *Hydrogeology Journal*, *10*(1), 52–67. https://doi.org/10.1007/s10040-001-0170-8
Stanley, E., Casson, N., Christel, S., Crawford, J., Loken, L., & Oliver, S. (2016). The ecology of methane in streams and rivers: Patterns, controls, and global significance. *Ecological Monographs*, *86*(2), 146–171. https://doi.org/10.1890/15-1027
Stumm, W., & Morgan, J. J. (1996). In J. L. Schnoor & A. Zehnder (Eds.), *Aquatic chemistry, chemical equilibria and rates in natural waters* (3rd ed.). John Wiley & Sons.
Teitelbaum, Y., Dallmann, J., Phillips, C. B., Packman, A. I., Schumer, R., Sund, N. L., et al. (2021). Dynamics of hyporheic exchange flux and fine particle deposition under moving bedforms. *Water Resources Research*, *57*(4), e2020WR028541. https://doi.org/10.1029/2020WR028541
Teitelbaum, Y., Shimony, T., Saavedra Cifuentes, E., Dallmann, J., Phillips, C. B., Packman, A. I., et al. (2022). A novel framework for simulating particle deposition with moving bedforms. *Geophysical Research Letters*, *49*(4), e2021GL097223. https://doi.org/10.1029/2021GL097223
Virtanen, P., Gommers, R., Oliphant, T. E., Haberland, M., Reddy, T., Cournapeau, D., et al. (2020). SciPy 1.0: Fundamental algorithms for scientific computing in Python. *Nature Methods*, *17*(3), 261–272. https://doi.org/10.1038/s41592-019-0686-2
Williams, P. J. l. B., & del Giorgio, P. A. (2005). Respiration in aquatic ecosystems: History and background. In P. del Giorgio & P. Williams (Eds.), *Respiration in aquatic ecosystems* (pp. 1–17). Oxford University Press.
Wolke, P., Teitelbaum, Y., Deng, C., Lewandowski, J., & Arnon, S. (2019). Impact of bed form celerity on oxygen dynamics in the hyporheic zone. *Water*, *12*(1), 62. https://doi.org/10.3390/w12010062
Zheng, L., Cardenas, M. B., Wang, L., & Mohrig, D. (2019). Ripple effects: Bed form morphodynamics cascading into hyporheic zone biogeochemistry. *Water Resources Research*, *55*(8), 7320–7342. https://doi.org/10.1029/2018WR023517
Zhou, T., & Endreny, T. A. (2013). Reshaping of the hyporheic zone beneath river restoration structures: Flume and hydrodynamic experiments. *Water Resources Research*, *49*(8), 5009–5020. https://doi.org/10.1002/wrcr.20384
Zlatanović, S., Fabian, J., Mendoza-Lera, C., Woodward, K. B., Premke, K., & Mutz, M. (2017). Periodic sediment shift in migrating ripples influences benthic microbial activity. *Water Resources Research*, *53*(6), 4741–4755. https://doi.org/10.1002/2017WR020656